



· 论 著 ·

基于多参数序列的儿童脑干弥漫性高级别胶质瘤临床影像学特征研究

陈 怡¹, 刘 明¹, 管文斌², 张培荣¹, 郑 慧¹, 张海波³

1. 上海交通大学医学院附属新华医院放射科, 上海 200092 ;

2. 上海交通大学医学院附属新华医院病理科, 上海 200092 ;

3. 上海交通大学医学院附属新华医院儿神经外科, 上海 200092

[摘要] 目的: 基于多参数序列探讨儿童脑干弥漫性高级别胶质瘤临床及影像学特征, 以提高对该病的全面认识。方法: 回顾并分析2022年1月—2024年1月就诊上海交通大学医学院附属新华医院并经病理学检查证实的儿童脑干弥漫性高级别胶质瘤的临床及影像学资料。结果: 共45例儿童脑干弥漫性高级别胶质瘤 [男性19例, 女性26例, 年龄(6.48 ± 2.34)岁] 纳入本研究, 其中4.4% (2/45) 出现脑脊液播散, 余脑干局限或附近浸润性生长。45例行计算机断层扫描 (computed tomography, CT) 平扫+磁共振成像 (magnetic resonance imaging, MRI) 平扫/增强扫描+弥散加权成像 (diffusion-weighted imaging, DWI) 基础扫描, 6例同时行CT灌注成像 (CT perfusion imaging, CTP) 扫描, 8例同时行磁共振波谱成像 (magnetic resonance spectroscopy, MRS) 扫描, 7例同时行弥散张量成像 (diffusion tensor imaging, DTI) 扫描, 2例同时行磁敏感加权成像 (susceptibility weighted imaging, SWI) 扫描。45例均内生性膨胀生长, 其中36例双侧均匀膨胀生长, 9例偏侧膨胀生长 (7例生长过程中越过中线, 2例单侧头尾端弥漫生长); 28.9% (13/45) 局限脑桥生长, 2.2% (1/45) 局限延髓生长, 68.9% (31/45) 向头尾端 (中脑/丘脑/延髓, 21/31, 67.7%) 和向侧方 (桥臂/小脑, 10/31, 32.3%) 生长, 26.7% (12/45) 进展为外生性 (其中11例包裹基底动脉, 11/12, 91.7%)。CT平扫序列显示脑干区域低密度增粗影, 密度低于正常脑干 ($P < 0.001$)。CT灌注序列扫描显示83.3% (5/6) 患者的肿瘤区域脑血流量 (cerebral blood flow, CBF) 降低 (1例显示肿瘤中心区域明显低于平均水平), 1例升高; 双侧大脑半球灌注异常, 达峰时间延迟, 以侧脑室周围为主。MRI结构序列显示肿瘤实性成分T1加权成像 (T1-weighted imaging, T1WI) 8.9% (4/45) 呈等信号、11.1% (5/45) 呈低信号, 80.0%呈混杂信号 (36/45), T2-液体抑制反转恢复 (fluid-attenuated inversion recovery, FLAIR) 序列呈稍高-高信号, T1WI增强后模式呈多样性改变, 6例不强化, 余不同程度轻-中度强化, 28.2% (11/39) 表现为局部环形强化、38.5% (15/39) 表现为局部结节状强化、10.3% (4/39) 表现为斑片状强化、23.1% (9/39) 表现为砂砾样强化、7.7% (3/39) 表现为混合模式强化, 部分T1WI增强不明显患者T2-FLAIR增强序列对比度更好。MRI功能序列中, MRS示Cho峰不同程度升高, NAA峰不同程度降低, 1例出现Lac峰明显倒置; DTI扫描显示病灶区神经纤维束被肿瘤推移至周边, 其中5例出现纤维束部分中断, 1例仅出现纤维束受压推挤。SWI相位图上可见局部呈低信号, 提示瘤内微出血。结论: 儿童脑干弥漫性高级别胶质瘤常规CT表现低密度脑干增粗, 量化有助于早期发现, 防止漏诊; 生长发生以弥漫内生性脑桥发生为主, 并多数沿神经纤维束方向浸润生长至其他脑区, 推移或破坏附近纤维束; 强化模式多样, 多表现为局部散在轻-中度强化; 内部可有囊变影像信号, 可能与局部灌注降低坏死、微出血后吸收等原因有关。

基金项目: 中国遗传资源保护与疾病防控教育部重点实验室开放课题 (LPHGRD2022-08)。

利益冲突: 无。

伦理批件: XHEC-D-2025-035。

知情同意: 有。

引用本文: 陈 怡, 刘 明, 管文斌, 等. 基于多参数序列的儿童脑干弥漫性高级别胶质瘤临床影像学特征研究 [J]. 肿瘤影像学, 2025, 34 (1): 72-78.

Funding: Open Project of Key Laboratory of Genetic Resources Protection and Disease Prevention and Control of the Ministry of Education in China (LPHGRD2022-08)

Conflicts of interest: no.

Ethical approval: XHEC-D-2025-035.

Informed consent: available.

Cite this article: CHEN Y, LIU M, GUAN W B, et al. Clinical imaging features of diffuse high-grade glioma in the brainstem of children based on multi-parameter sequences [J]. Oncoradiology, 2025, 34(1): 72-78.

[关键词] 脑干; 弥漫性胶质瘤; 磁共振成像; 儿童

中图分类号: R739.41; R445.2 文献标志码: A

DOI: 10.19732/j.cnki.2096-6210.2025.01.010

Clinical imaging features of diffuse high-grade glioma in the brainstem of children based on multi-parameter sequences CHEN Yi¹, LIU Ming¹, GUAN Wenbin², ZHANG Peirong¹, ZHENG Hui¹, ZHANG Haibo³ (1. Department of Radiology, Xinhua Hospital, Shanghai Jiao Tong University School of Medicine, Shanghai 200092, China; 2. Department of Pathology, Xinhua Hospital, Shanghai Jiao Tong University School of Medicine, Shanghai 200092, China; 3. Department of Pediatric Neurosurgery, Xinhua Hospital, Shanghai Jiao Tong University School of Medicine, Shanghai 200092, China)

Correspondence to: ZHANG Haibo E-mail: kexue168163@163.com

[Abstract] **Objective:** To explore the clinical and imaging features of diffuse high-grade gliomas in the brainstem of children based on multi parameter sequences, so as to improve the comprehensive understanding of the disease. **Methods:** The clinical and imaging data of pediatric brain stem diffuse high-grade gliomas confirmed by pathology from January 2022 to January 2024 were retrospectively analyzed. **Results:** A total of 45 children in Xinhua Hospital, Shanghai Jiao Tong University School of Medicine with diffuse high-grade gliomas in the brainstem (19 males and 26 females, aged 6.48 ± 2.34 years) were included in this study. Among them, 4.4% (2/45) had cerebrospinal fluid dissemination, while the rest had localized or nearby infiltration and growth in the brainstem. 45 cases underwent computed tomography (CT) plain scan+ magnetic resonance imaging (MRI) plain scan/enhanced scan+diffusion-weighted imaging (DWI) basic scan, 6 cases underwent CT perfusion imaging (CTP) scan simultaneously, 8 cases underwent magnetic resonance spectroscopy (MRS) scan simultaneously, 7 cases underwent diffusion tensor imaging (DTI) scan simultaneously, and 2 cases underwent susceptibility weighted imaging (SWI) scan simultaneously. All 45 cases had endogenous swelling growth, including 36 cases with uniform swelling growth on both sides and 9 cases with lateral swelling growth (7 cases crossed the midline during the growth process, and 2 cases with diffuse growth on one side of the head and tail); 28.9% (13/45) limited brainstem growth, 2.2% (1/45) limited medullary growth, 68.9% (31/45) grew towards the head and tail (midbrain/thalamus/medulla oblongata, 21/31, 67.7%) and laterally (pons/cerebellum, 10/31, 32.3%), and 26.7% (12/45) progressed to exogeneity (including 11 cases involving the basilar artery, 11/12, 91.7%). The CT plain scan sequence showed low-density thickening shadows in the brainstem area, with a density lower than that of the normal brainstem ($P < 0.001$). CT perfusion sequence scan showed a decrease in cerebral blood flow (CBF) in the tumor area of 83.3% (5/6) of patients (1 case showed a significantly lower than average level in the tumor center area), and 1 case showed an increase. Bilateral cerebral hemisphere perfusion abnormalities, with delayed peak time, mainly around the lateral ventricles. The MRI structural sequence showed that 8.9% (4/45) of the tumor solid components on T1-weighted imaging (T1WI) showed equal signal intensity, 11.1% (5/45) showed low signal intensity, and 80.0% showed mixed signal intensity (36/45). The T2-fluid suppressed inversion recovery (FLAIR) sequence showed slightly high to high signal intensity, and the pattern after T1WI enhancement showed diverse changes. Six cases did not show enhancement, while the rest showed varying degrees of mild to moderate enhancement. 28.2% (11/39) showed local circular enhancement, 38.5% (15/39) showed local nodular enhancement, 10.3% (4/39) showed patchy enhancement, and 23.1% (9/39) showed patchy enhancement. Manifested as gravel like enhancement, 7.7% (3/39) showed mixed mode enhancement, and some patients with unclear T1WI enhancement had better T2-FLAIR enhancement sequence contrast. In the MRI functional sequence, MRS showed varying degrees of increase in Cho peak and decrease in NAA peak, with one case showing a significant inversion of Lac peak; DTI scan showed that the nerve fiber bundles in the lesion area were pushed to the periphery by the tumor, with 5 cases showing partial interruption of the fiber bundles and 1 case only showing compression and pushing of the fiber bundles. Local low signal can be seen on the SWI phase map, indicating intratumoral microbleeds. **Conclusion:** The conventional CT findings of diffuse high-grade gliomas in the brain stem of children are low-density brain stem thickening, and quantification is helpful for early detection and prevention of missed diagnosis. The growth mainly occurred in the diffuse endogenous pontine, and most of them infiltrated and grew to other brain regions along the direction of nerve fiber bundles, pushing or destroying the nearby fiber bundles. The enhancement patterns were various, and most of them were scattered mild to moderate enhancement. There may be cystic image signals inside, which may be related to the reduction of necrosis by local perfusion and absorption after microbleeds;

[Key words] Brainstem; Diffuse glioma; Magnetic resonance imaging; Children

儿童弥漫性脑肿瘤预后较局限性脑肿瘤预后差,常分为弥漫性低级别胶质瘤和儿童弥漫性高级别胶质瘤两种类型,2021年第五版世界卫生组织(World Health Organization, WHO)儿童中枢神经系统弥漫性高级别胶质瘤肿瘤分类中新增“H3K27M突变型,弥漫性中线胶质瘤”,也是儿童中高发病理学类型,呈弥漫性/浸润性生长,预后差,好发于脑干,也散在发生其他部位包括丘脑、松果体、小脑和脊髓等中线结构处^[1]。本研究回顾并分析发生于脑干的儿童弥漫性高级别胶质瘤的临床及影像学资料,研究其影像学特征及生长方式,以期提高对其临床、影像的全面认识。

1 资料和方法

1.1 研究对象

回顾并分析2022年1月—2024年1月就诊于上海交通大学医学院附属新华医院经临床病理学检查证实的儿童脑干弥漫性高级别胶质瘤的临床及影像学资料。纳入标准:①经术后病理学检查证实,临床及病理学资料完整的初发患者;②术前影像学资料完整,无明显伪影。排除标准:①术前接受过手术或其他辅助治疗(如放疗);②图像质量无法满足后续研究。

1.2 检查方法

所有患者术前均行计算机体层成像(computed tomography, CT)平扫+磁共振成像(magnetic resonance imaging, MRI)平扫/增强扫描。

平扫序列包括T1-液体抑制反转恢复(fluid attenuated inversion recovery, FLAIR)序列,重复时间(repetition time, TR)1 800 ms,回波时间(echo time, TE)20 ms,层厚5 mm,间隔6 mm;T2-FLAIR序列,TR 7 000 ms,TE 120 ms,层厚5 mm,间隔6 mm,增强对比剂使用Gd-DTPA(0.1 mmol/kg)^[2]。部分患者加做其他影像学序列扫描。CT灌注成像(computed tomography perfusion imaging, CTP)采用德国

Siemens公司的Definition AS 64排螺旋CT机进行检查,扫描参数:矩阵512×512,视野320 mm×320 mm。MRI检查采用荷兰Philips公司的Ingenia 3.0 T CX扫描仪,弥散加权成像(diffusion-weighted imaging, DWI)采用单激发平面回波成像序列,TR 8 000~10 000 ms,TE 70~100 ms,轴位成像,按各向同性施加弥散敏感梯度磁场, b 值取0和1 000 s/mm²,层厚5 mm,间隔1 mm,视野15~30 cm,矩阵256×128,激励次数为2次。磁共振波谱成像(magnetic resonance spectroscopy, MRS)采用单体素,体素大小为2 cm×2 cm×2 cm,选择肿瘤明显强化区域或实性区域为感兴趣区,同时尽可能避开骨骼、脂肪、脑脊液、肿瘤坏死、囊变部分。弥散张量成像(diffusion tensor imaging, DTI)扫描参数: b 值为0和1 000 s/mm²,弥散编码向量沿32个非平行方向,TR 14 000 ms,TE 76.9 ms,层厚2.5 mm,间距0 mm,视野24.0 cm×16.8 cm,矩阵96×96,激励次数1。磁敏感加权成像(susceptibility weighted imaging, SWI):TR 55.2 ms,TE 5.3 ms,层厚1.2 mm,视野22 cm×22 cm,矩阵320×288,激励次数0.75。通过SWI后处理软件自动得到校正的相位图和幅度图,再对幅度图进行最小密度投影得到MinP图。

1.3 影像学征象分析

由2名经验丰富的放射科主治医师独立评价及处理图像,评价内容包括肿瘤部位、浸润方向,CT密度高低(包括CT值提取),CTP后处理及数据提取,MRI结构序列信号强弱、增强后模式(强化程度和强化形态),MRI功能序列(DWI、MRS、DTI、SWI)后处理及数据提取。

1.4 统计学处理

采用SPSS 18.0统计学软件进行分析,符合正态分布的计量资料采用 $\bar{x}\pm s$ 描述,两组间比较采用独立样本 t 检验;不符合正态分布者以 $M(P_{25}, P_{75})$ 表示,两组间比较采用Mann-Whitney U 检验。计数资料以 $n(\%)$ 表示,组间比较采用 χ^2 检验。 $P<0.05$ 为差异有统计学意义。

2 结 果

共45例儿童脑干弥漫性高级别胶质瘤纳入本研究，其中男性19例，女性26例，年龄 (6.48 ± 2.34) 岁（图1）。临床上都伴有高级思

维活跃度降低和运动功能障碍（包括走路不稳、单侧或双侧肢体活动障碍、眼球活动异常、饮水呛咳、共济失调等）。术前均行CT平扫+MRI平扫/增强扫描+DWI基础扫描，6例同时行CTP扫描，8例同时行MRS扫描，7例同时行DTI扫描，2例同时行SWI扫描。

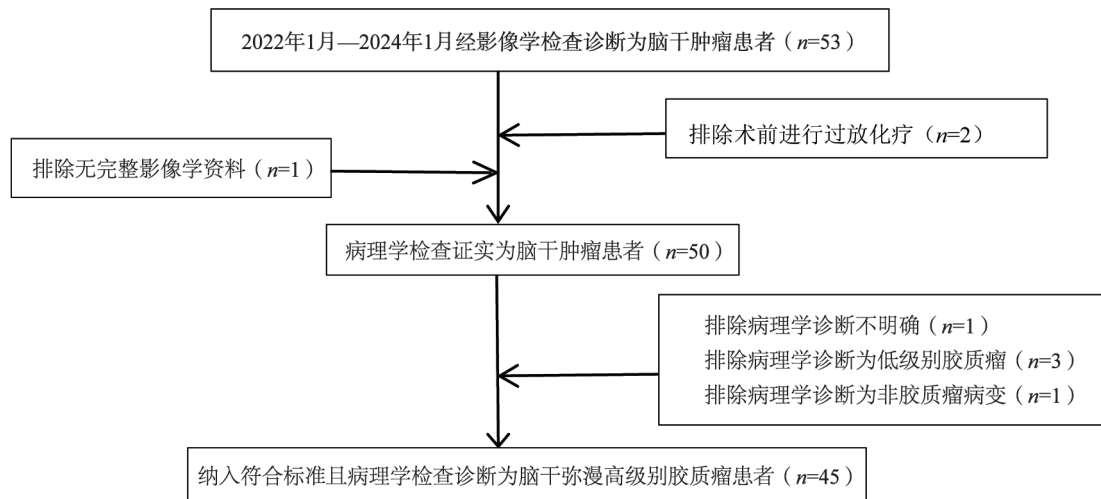


图1 研究对象纳入流程图

Fig.1 Flow chart for inclusion of participants

全部患者病灶均内生性膨胀生长，其中36例双侧均匀膨胀生长，9例偏侧膨胀生长（7例生长过程中越过中线，2例单侧头尾端弥漫生长）；2例（4.4%）出现脑脊液播散，余脑干局限或附近浸润性生长，其中28.9%（13/45）局限脑桥生长，2.2%（1/45）局限延髓生长，68.9%（31/45）向头尾端（中脑/丘脑/延髓，67.7%）和向侧方（桥臂/小脑，10/31，32.3%）生长，26.7%（12/45）进展为外生性（其中11例包裹基底动脉，91.7%）。CT平扫序列显示脑干区域低密度增粗影，CT值 (24.18 ± 5.84) 低于正常脑干 (31.45 ± 1.23) ， $P < 0.001$ 。CTP扫描显示83.3%（5/6）患者的肿瘤区域CBF降低（1例显示肿瘤中心区域明显低于平均水平），1例升高；双侧大脑半球灌注异常，达峰时间延迟，以侧脑室周围为主（图2）。

MRI结构序列显示肿瘤实性成分T1加权成像（T1-weighted imaging, T1WI）呈等（4/45，8.9%）、低（5/45，11.1%）及混杂信号

（36/45，80.0%），T2-FLAIR呈稍高-高信号，T1WI增强后模式呈多样性改变，6例不强化，余不同程度轻-中度强化，表现为局部环形强化（11/39，28.2%）、局部结节状强化（15/39，38.5%）、斑片状强化（4/39，10.3%）、砂砾样强化（9/39，23.1%）和混合模式强化（3/39，7.7%）。2例（2/45，4.4%）出现脑脊液播散，表现为双侧脑室周围区域和侧脑室前角的脑室内结节，提示软脑膜和室管膜下种植。1例T1WI增强不明显患者行T2-FLAIR增强序列扫描，相对于T1WI弱增强，T2-FLAIR增强序列中可呈现更为明显的强化表现（图3）。

MRI功能序列中，DWI示肿瘤呈整体或局部高/稍高信号（23/45，51.1%）和等-低信号（22/45，48.9%）。MRS示Cho峰不同程度升高，NAA峰不同程度降低，Cho/Cr为1.14~3.97，Cho/NAA为1.05~25.6，1例出现Lac峰明显倒置，1例术前MRI结构序列怀疑脑干脑炎，后MRS显示NAA峰减低，Cho峰升高。

Cho/Cr为1.15, Cho/NAA为1.67, NAA/Cr为0.687; 对于均匀膨胀生长患者进行DTI扫描, 显示病灶区神经纤维束被肿瘤推移至周边, 其中

5例出现纤维束部分中断, 1例仅出现纤维束受压推挤。SWI相位图上可见局部呈低信号, 提示瘤内微出血。

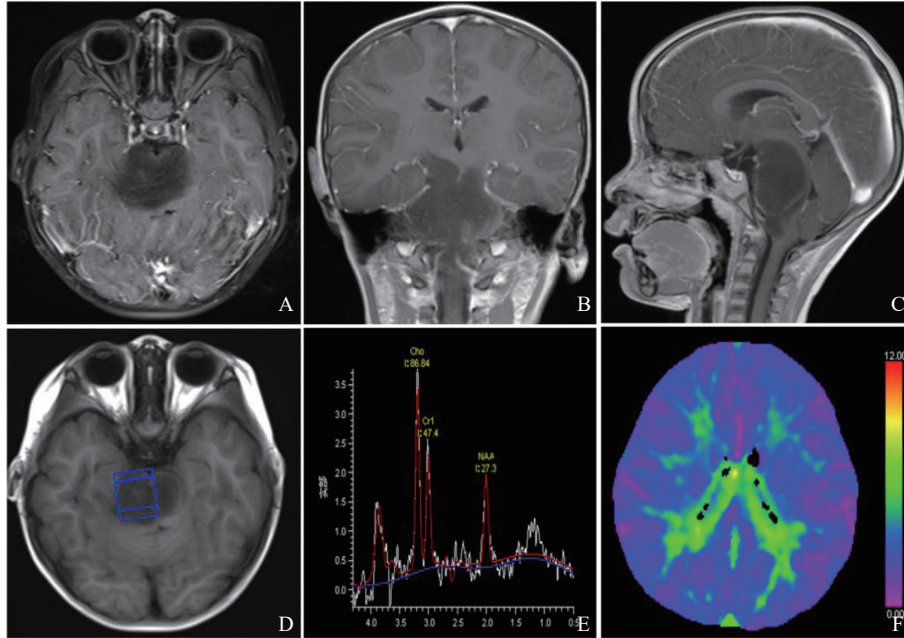


图2 脑干高级别胶质瘤的多模态影像学图像

Fig.2 Multi-modal imaging of high-grade glioma in the brainstem

A: 轴位增强后; B: 冠状位增强后; C: 矢状位增强后; D: MRS区域选择; E: MRS显示Cho峰升高, NAA峰降低; F: CT灌注显示侧脑室周围降低明显。

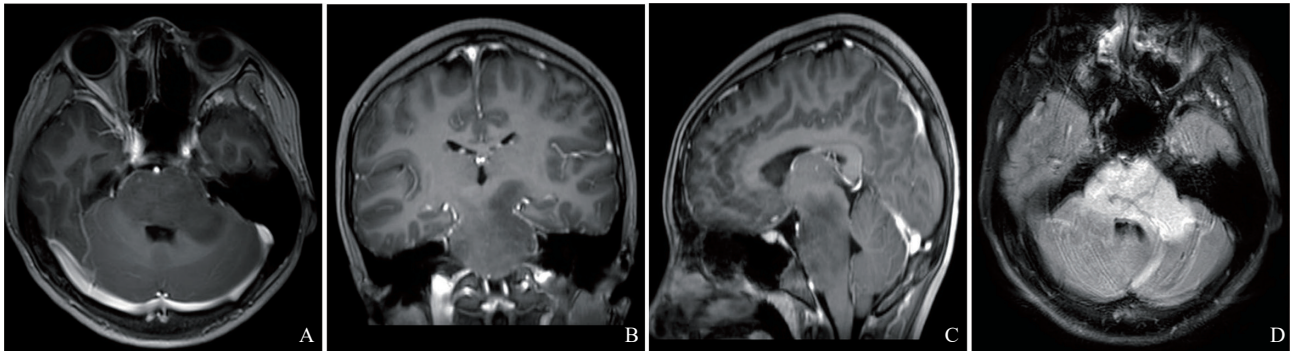


图3 脑干高级别胶质瘤的多序列图像

Fig.3 Images of high-grade gliomas in the brainstem

A: 常规T1WI增强后轴位显示强化不明显; B: 增强后冠状位; C: 增强后矢状位; D: T2-FLAIR增强后清晰显示肿瘤大小及表面血管。

3 讨 论

2021年第五版WHO儿童中枢神经系统弥漫性高级别胶质瘤分类中包括弥漫性中线胶质瘤(伴有H3K27变异)、弥漫性半球胶质瘤(伴有

H3G34变异)、弥漫性高级胶质瘤(H3和IDH野生型)和婴儿型半球胶质瘤^[2]。弥漫性中线胶质瘤主要发生于儿童和青少年,也可能发生于成年人。这些病变通常位于中线结构(脑干、丘脑和脊髓),其组蛋白H3的第27位赖氨酸被蛋氨酸所取代,这一改变导致H3K27三甲基化的整体

减少, H3K27乙酰化增加, 最终驱动广泛的致癌基因改变, 加速弥漫性中线神经胶质瘤的恶性进展。该类肿瘤侵袭性高, 预后较差, 2年生存率<10%, 系统全面的影像学研究对临床评估具有重要的指导意义。

MRS中的部分代谢产物与肿瘤生物学分级及患者预后密切相关, 如较高的Cho(胆碱)水平与较短的总生存期及无进展生存期相关^[3], Cho/Cr(肌酸)和神经胶质瘤分级之间存在正相关, NAA(N-乙酰天冬氨酸)/Cr或NAA/Cho与神经胶质瘤分级之间呈负相关^[4]。本研究中MRS示Cho峰不同程度升高, NAA峰不同程度降低, 反映肿瘤细胞增殖活跃, 符合高级别胶质瘤生物学特性, 可以作为术前鉴别诊断(如脑干脑炎)的重要手段, 该特性导致其生长迅速, 内部缺血缺氧区常发生囊变、坏死、微出血等病理学改变, 这些通过其他MRI功能序列可以提示, 如DWI上局部囊变呈高信号, 弥散受限, SWI相位图上局部呈低信号, 提示瘤内微出血, CT灌注肿瘤中心区域CBF明显降低等。反映在MRI结构序列上表现为各序列信号混杂, T1WI呈等、低及混杂信号, T2-FLAIR呈稍高-高信号, 给药后不强化或轻-中度强化, 外观上表现为局部环形强化、局部结节状强化、斑片状强化、砂砾样强化和混合模式强化。部分患者T1WI呈等信号, 给药后不强化^[5-6], 组织病理Ki-67增殖指数不高, 容易误诊为低级别胶质瘤, 但是, 根据WHO分类标准, 如有H3K27M变异, 预后较差, 仍归类为高级别胶质瘤, 此时, 相对于T1WI强化表现不明显的患者, T2-FLAIR增强序列对低浓度钆更敏感, 病灶显示更好^[7-8]。

脑干高级别胶质瘤软脑膜和室管膜下播散并不常见, 但也并不罕见, 常被视为癌症进展或复发的晚期并发症^[9], 因此, 脑干胶质瘤在放疗前和放疗后, 都有必要进行全神经轴MRI评估, 以便更好地制订放疗计划和全面地评估病情进展。软脑膜播散在脑干高级别胶质瘤初诊时很少观察到, 但随着肿瘤进展, 发病率增加, 影像学上可表现为沿侧脑室和第三脑室的室管膜表面延伸的T2-FLAIR高信号肿块, 弥漫性软脑(脊)

膜增强^[10], 如同时伴有体温波动等, 容易误诊为中枢神经系统感染^[11], 本研究中1例临床进展迅速, 术前考虑脑干脑炎, 多模态影像学评估及活检病理显示非常重要。

脑桥臂又称小脑中脚, 参与控制随意运动, 肿瘤浸润小脑中脚可导致运动功能障碍, 表现为走路不稳, 共济失调等, Makepeace等^[12]发现脑干高级别胶质瘤浸润小脑中脚的患者生存时间短、预后差。本研究(69%)及既往研究^[13]均显示, 肿瘤多向脑桥外脑区(如小脑中脚、丘脑、基底节区等)浸润生长, 弥漫性脑桥胶质瘤中各向异性和轴向弥散率的降低以及径向弥散率的增加可能反映了肿瘤沿皮质脊髓束的扩展, DTI可以在常规MRI结构序列变得明显之前早期检测到肿瘤远处扩展。Wang等^[14]从分子生物学机制方面探讨了Notch1-Sox9-Sox2正反馈环路、RhoA-ROCK-SPARC信号通路、肿瘤微环境中神经胶质瘤网络、肿瘤微管、神经胶质瘤和周围细胞之间的间隙连接等都在胶质瘤沿着神经纤维束浸润生长中发挥着重要作用。这种亲纤维性导致其侵袭方向沿着纤维束走行, 本组中2例沿着头尾侧方向进展(平行纤维束方向), 而没有越过中线(垂直纤维束方向), 此外, 亲纤维性也导致纤维束破坏, 进而影响高级认知功能^[15]。Cheng等^[16]使用静息态功能磁共振成像(rs-fMRI)研究弥漫性内生型桥脑胶质瘤(DIPG)患者的局部神经功能改变, 研究包括17例DIPG患者(8例儿童有行为抑制缺陷, 9例儿童没有行为抑制缺陷)和5名基线水平一致的健康儿童作为对照, 结果显示行为抑制组患者的低频振幅(amplitude of low-frequency fluctuation, ALFF)在左背外侧额上回和右梭状回等脑区表现出显著差异, 而在左边缘上回、左额中回和右内侧额上回等脑区表现出ALFF升高。Jia等^[17]对146例儿童脑干肿瘤患者通过行为量表评估他们的行为和情绪, 结果显示脑干肿瘤患儿表现出严重的行为和情绪问题, 位于脑桥或位于中脑的DIPG是神经精神症状的重要风险因素, 尤其在孤僻、焦虑/抑郁症状、思维问题、注意力缺陷、外化问题和攻击行为等方面, 脑桥肿瘤患者

的得分明显高于延髓肿瘤患者。在本研究中, 通过CTP发现, 侧脑室周围达峰时间延迟, 提示可能神经纤维束区域缺血, 与DTI上神经纤维破坏互为补充, 具体机制待进一步研究, 此外, 通过CTP也可以为后续抗血管生成治疗灵敏度提供佐证^[18]。

综上所述, 儿童脑干弥漫性高级别胶质瘤病理异质性强, 通过影像学多参数序列评估可以全面地评估患儿临床症状背后的病理生理学机制, 为治疗手段的选择提供帮助。

第一作者:

陈 怡 (ORCID: 0009-0002-7610-4474), 本科, 技师, E-mail: zhengxiaoyi@163.com

通信作者:

张海波 (ORCID: 0009-0009-8485-644X), 博士, 主治医师, E-mail: kexue168163@163.com

作者贡献说明:

陈怡: 提出论文基本框架、提出研究方向、设计论文框架, 撰写论文, 获得项目支持; 刘明: 处理性数据; 管文斌: 采集与分析数据; 张培荣、郑慧: 参与数据采集与分析; 张海波: 参与论文起草、修订、审核, 论文最终版本修订。

[参 考 文 献]

- [1] 赵 玮, 郑 慧, 夏正荣, 等. 儿童颅内混合性生殖细胞肿瘤临床及影像学表现 [J]. 中国临床医学影像杂志, 2023, 34(3): 169-174.
ZHAO W, ZHENG H, XIA Z R, et al. Clinical and imaging features of pediatric intracranial mixed germ cell tumor [J]. J China Clin Med Imag, 2023, 34(3): 169-174
- [2] LOUIS D N, PERRY A, WESSELING P, et al. The 2021 WHO classification of tumors of the central nervous system: a summary [J]. Neuro Oncol, 2021, 23(8): 1231-1251.
- [3] SHI Y X, LIU D L, KONG Z R, et al. Prognostic value of choline and other metabolites measured using ¹H-magnetic resonance spectroscopy in gliomas: a meta-analysis and systemic review [J]. Metabolites, 2022, 12(12): 1219.
- [4] YAO R, CHENG A L, LIU M L, et al. The diagnostic value of apparent diffusion coefficient and proton magnetic resonance spectroscopy in the grading of pediatric gliomas [J]. J Comput Assist Tomogr, 2021, 45(2): 269-276.
- [5] 丁 茗, 郑 慧, 冯 赟, 等. 儿童弥漫性中线胶质瘤伴 *H3K27M* 突变MRI表现 [J]. 实用放射学杂志, 2020, 36(3): 444-447.
DING M, ZHENG H, FENG Y, et al. MRI characteristics of diffuse midline gliomas with *H3K27M* mutation in children [J]. J Pract Radiol, 2020, 36(3): 444-447.
- [6] 张亚莹, 肖 慧, 杨 涛, 等. *H3K27M* 突变型弥漫性中线胶质瘤MRI表现 [J]. 临床放射学杂志, 2021, 40(1): 16-20.
ZHANG Y Y, XIAO H, YANG T, et al. MRI manifestations of diffuse midline gliomas with histone *H3K27M* mutation [J]. J Clin Radiol, 2021, 40(1): 16-20.
- [7] 曹明慧, 苏 赟, 苏卫锋, 等. 钆对比剂剂量对增强T2 FLAIR序列与增强T1WI序列脑转移瘤强化效果的影响及对比研究 [J]. 磁共振成像, 2024, 15(1): 152-157.
CAO M H, SU Y, SU W F, et al. Comparative study of different doses of gadolinium contrast agent on contrast enhanced T2 FLAIR and T1WI in diagnosis of brain metastases [J]. Chin J Magn Reson Imag, 2024, 15(1): 152-157.
- [8] AHN S J, TAOKA T, MOON W J, et al. Contrast-enhanced fluid-attenuated inversion recovery in neuroimaging: a narrative review on clinical applications and technical advances [J]. J Magn Reson Imaging, 2022, 56(2): 341-353.
- [9] WEGENER E, HORSLEY P, WHEELER H, et al. Leptomeningeal neuraxis relapse in glioblastoma is an uncommon but not rare event associated with poor outcome [J]. BMC Neurol, 2023, 23(1): 328.
- [10] NAVARRO R E, GOLUB D, HILL T, et al. Pediatric midline *H3K27M*-mutant tumor with disseminated leptomeningeal disease and glioneuronal features: case report and literature review [J]. Childs Nerv Syst, 2021, 37(7): 2347-2356.
- [11] LEE J K, KO H C, CHOI J G, et al. A case of diffuse leptomeningeal glioneuronal tumor misdiagnosed as chronic tuberculous meningitis without brain biopsy [J]. Case Rep Neurol Med, 2018, 2018: 1391943.
- [12] MAKEPEACE L, SCOGGINS M, MITREA B, et al. MRI patterns of extrapontine lesion extension in diffuse intrinsic pontine gliomas [J]. AJNR Am J Neuroradiol, 2020, 41(2): 323-330.
- [13] WAGNER M W, ROBERT BELL W, KERN J, et al. Diffusion tensor imaging suggests extrapontine extension of pediatric diffuse intrinsic pontine gliomas [J]. Eur J Radiol, 2016, 85(4): 700-706.
- [14] WANG J, YI L, KANG Q M, et al. Glioma invasion along white matter tracts: a dilemma for neurosurgeons [J]. Cancer Lett, 2022, 526: 103-111.
- [15] ANDREOLI M, MACKIE M A, AABY D, et al. White matter tracts contribute selectively to cognitive functioning in patients with glioma [J]. Front Oncol, 2023, 13: 1221753.
- [16] CHENG X, GAO P Y. Abnormal neural activity in children with diffuse intrinsic pontine glioma had manifested deficit in behavioral inhibition: a resting-state functional MRI study [J]. J Comput Assist Tomogr, 2019, 43(4): 547-552.
- [17] JIA H Y, ZHANG P, GU G C, et al. Brainstem tumors may increase the impairment of behavioral emotional cognition in children [J]. J Neurooncol, 2022, 160(2): 423-432.
- [18] EVANS M, GILL R, BULL K S. Does a Bevacizumab-based regime have a role in the treatment of children with diffuse intrinsic pontine glioma? A systematic review [J]. Neurooncol Adv, 2022, 4(1): vdac100.

(收稿日期: 2024-10-12 修回日期: 2024-12-24)